


Nanoparticles targeting immune checkpoint protein VISTA induce potent antitumor immunity

Taylor J Moon,¹ Hieu Minh Ta,² Anubhuti Bhalotia,¹ Kai E Paulsen,¹ Diarmuid W Hutchinson,¹ Gabrielle M Arkema,¹ Andrew S Choi,¹ Michiko G Haynie,¹ Laolu Ogunnaike,¹ Margee Dever,¹ Li Lily Wang,^{1,2,3} Efstathios Karathanasis ^{1,4}

To cite: Moon TJ, Ta HM, Bhalotia A, *et al.* Nanoparticles targeting immune checkpoint protein VISTA induce potent antitumor immunity. *Journal for ImmunoTherapy of Cancer* 2024;**12**:e008977. doi:10.1136/jitc-2024-008977

► Additional supplemental material is published online only. To view, please visit the journal online (<https://doi.org/10.1136/jitc-2024-008977>).

TJM and HMT contributed equally.

LLW and EK are joint senior authors.

Accepted 12 August 2024



© Author(s) (or their employer(s)) 2024. Re-use permitted under CC BY-NC. No commercial re-use. See rights and permissions. Published by BMJ.

For numbered affiliations see end of article.

Correspondence to
Professor Efstathios Karathanasis; stathis@case.edu

Dr Li Lily Wang; wangl9@ccf.org

ABSTRACT

Background Immune checkpoint protein V-domain immunoglobulin suppressor of T cell activation (VISTA) controls antitumor immunity and is a valuable target for cancer immunotherapy. Previous mechanistic studies have indicated that VISTA impairs the toll-like receptor (TLR)-mediated activation of myeloid antigen-presenting cells, promoting the expansion of myeloid-derived suppressor cells, and suppressing tumor-reactive cytotoxic T cell function.

Methods The aim of this study was to develop a dual-action lipid nanoparticle (dual-LNP) coloaded with VISTA-specific siRNA and TLR9 agonist CpG oligonucleotide. We used three murine preclinical tumor models, melanoma YUMM1.7, melanoma B16F10, and colon carcinoma MC38 to assess the functional synergy of the two cargoes of the dual LNP and therapeutic efficacy.

Results The dual-LNP synergistically augmented antitumor immune responses and rejected large established tumors whereas LNPs containing VISTA siRNA or CpG alone were ineffective. In comparison with therapies using the soluble CpG and a VISTA-specific monoclonal antibody, the dual-LNP demonstrated superior therapeutic efficacy yet with reduced systemic inflammatory cytokine production. In three murine models, the dual-LNP treatment achieved a high cure rate. Tumor rejection was associated with influx of immune cells to tumor tissues, augmented dendritic cell activation, production of proinflammatory cytokines, and improved function of cytotoxic T cells.

Conclusions Our studies show the dual-LNP ensured codelivery of its synergistic cargoes to tumor-infiltrating myeloid cells, leading to simultaneous silencing of VISTA and stimulation of TLR9. As a result, the dual-LNP drove a highly potent antitumor immune response that rejected large aggressive tumors, thus may be a promising therapeutic platform for treating immune-cold tumors.

BACKGROUND

Cancer immunotherapy aims to induce the activation of both innate and adaptive immunity, leading to a potent antitumor response against cancerous cells.^{1,2} Clinically successful immunotherapies require robust engagement of cytotoxic T lymphocytes (CTLs) that

WHAT IS ALREADY KNOWN ON THIS TOPIC

- ⇒ Immune checkpoint protein V-domain immunoglobulin suppressor of T cell activation (VISTA) controls antitumor immunity and is a valuable target for cancer immunotherapy.
- ⇒ VISTA impairs the toll-like receptor (TLR)-mediated activation of myeloid antigen-presenting cells, promoting the expansion of myeloid-derived suppressor cells, and suppressing tumor-reactive cytotoxic T cell function.

WHAT THIS STUDY ADDS

- ⇒ This study reports the design of a dual-action nanoparticle that ensures the codelivery of two synergistic cargoes to tumor-associated myeloid cells leading to potent antitumor immune responses due to simultaneous gene silencing of VISTA and stimulation of TLR9.
- ⇒ In comparison with therapies using the soluble TLR9 agonist CpG and a VISTA-specific monoclonal antibody, the dual lipid nanoparticle demonstrated superior therapeutic efficacy yet with reduced systemic inflammatory cytokine production.

HOW THIS STUDY MIGHT AFFECT RESEARCH, PRACTICE OR POLICY

- ⇒ This study demonstrates the feasibility, safety, and efficacy of a nanoparticle vaccine targeting a critical immune checkpoint protein VISTA for cancer immunotherapy.

seek out and eliminate tumor cells. However, the massive immunosuppression perpetuated in the tumor microenvironment (TME) poses a significant challenge to these immunotherapies as tumor-specific CTLs are often marginalized and excluded from cancer masses.^{3–5} Therefore, successful immunotherapy regimes seek to induce or improve cytotoxic antitumor responses.

The B7 family of immune checkpoint receptors (ICRs) is highly valuable targets for cancer immunotherapy.⁶ Antibodies

targeting two B7 family coinhibitory receptors CTLA-4 and PD-1 have elicited durable clinical outcomes in previously refractory cancer types and are considered a breakthrough therapy for cancer.^{7,8} In addition to CTLA-4 and PD-L1/PD-1 pathways, several additional ICRs, including V-domain immunoglobulin suppressor of T cell activation (VISTA), TIGIT, LAG3, and TIM3 play nonredundant roles in impairing antitumor immunity.⁶ The development of novel therapeutics targeting these next-generation ICRs may significantly advance the field of cancer immunotherapy.

VISTA (gene *Vsir*, also known as *Gi24*, *Dies-1*, *PD-1H*, and *DD1*) stands for V domain immunoglobulin suppressor of T cell activation and is an established B7 family ICR.^{9,10} Studies from our group and others have shown that VISTA impairs antitumor immunity.^{9,11} Mechanistically, VISTA plays a broader role in regulating both T cell-mediated and myeloid cell-mediated antitumor responses.⁹⁻¹⁷ The T-cell suppressive action of VISTA has been attributed to engagement of coinhibitory receptors, including *LRIG1* and *PSGL-1* in T cells.^{12,18} Another study demonstrated T cell-intrinsic inhibitory function of VISTA.⁹ On the other hand, VISTA is also highly expressed in antigen-presenting cells (APCs), including dendritic cells (DCs) and macrophages. VISTA downregulates the signaling responses following TLR stimulation in myeloid APCs and reduces the production of T cell-stimulatory cytokines such as IL-12 and IL-27.^{10,19} In both melanoma and colon cancer models, treatment with VISTA-specific monoclonal antibody (mAb) elevated the expression of MHC class II and genes involved in antigen presentation (ie, IL-12, CD80, etc) in tumor-infiltrating monocyte-derived DCs.^{16,20} In addition to APCs, VISTA is also expressed in tumor-associated myeloid-derived suppressor cells (MDSCs) and promote MDSC differentiation and suppressive function.²¹ Blocking VISTA by gene deletion or using antibodies partially ablated the suppressive effects of M-MDSCs.^{19,21,22} In murine tumor models such as melanoma and colon cancer models, treatment with a VISTA-specific mAb synergized with TLR agonists and elicited superior therapeutic efficacies.¹⁹

Despite the immunostimulatory effects of VISTA inhibition, systemic treatment with VISTA-blocking antibodies triggered significant production of inflammatory cytokines (ie, IL-6, IL-12, and TNF- α .) in the periphery, which may exacerbate the cytokine release syndrome and immune-related adverse events (irAEs).¹⁹ In this context, irAEs are commonly associated with immune checkpoint inhibitors (ICIs) that target CTLA4 and PD-L1/PD-1 pathways and are partly contributed by cytokines such as IL-1 and IL-6.²³ Thus, alternative strategies to block VISTA while minimizing systemic cytokine release may be more advantageous in the context of clinical applications.

Based on the previous studies showing that VISTA-specific mAb synergized with TLR agonists,¹⁹ we rationalize that a therapeutic nanoparticle with dual activity may be effective in treating aggressive and immune-cold tumors. To test this hypothesis, we developed the

dual-lipid nanoparticle (LNP) codelivering VISTA-specific siRNA and the TLR9 agonist CpG. First, gene silencing is a promising alternative approach to antibody-mediated immunotherapy. One of the main advantages of gene silencing is the more durable knockout of the target protein.²⁴⁻²⁶ LNP can efficiently deliver nucleotide-based therapies by using ionizable cationic lipids that ionically bind and encapsulate the negatively charged siRNA molecules and CpG dinucleotides.^{27,28} The dual-LNP facilitates highly stable and efficient entrapment of the two nucleotide-based therapies, provides protection of its cargoes from degradation, diminished immunogenicity, low toxicity, and mediates proficient delivery of cargo to myeloid cells in a tumor. Intratumoral (IT) administration of dual-LNP ensures the simultaneous delivery of its two synergistic cargoes and uptake by the same tumor-associated myeloid cell, thus achieving optimal effects to activate these cells. An additional benefit of the IT administration of dual-LNP is the reduced systemic proinflammatory effects, in comparison to soluble TLR9 agonist or VISTA mAb. Using three murine preclinical tumor models, YUMM1.7, B16F10, and MC38 tumor models, we show that the dual-LNP vaccine induced high rate of rejection of large, pre-established tumors and that tumor clearance was associated with reprogramming of the immunosuppressive myeloid cells and improved function of CD8⁺ CTLs. In addition to primary tumor rejection, dual-LNP also resulted in an effective immunological memory against tumor recurrence.

METHODS

LNP synthesis

LNP formulations were made with D-Lin-MC3 ionizable cationic lipid (Cayman Chemical), distearoylphosphatidylcholine (DSPC) (Avanti Lipids), cholesterol-ovine (Avanti Lipids), 1,2-dimyristoyl-rac-glycero-3-methoxy polyethylene glycol-2000 (DMG-PEG2000) (Avanti Lipids) and 1,2-Distearoyl-sn-glycero-3-phosphoethanolamine-mPEG (DSPE-mPEG2000) (Laysan Bio) at a molar ratio of 50:10.5:38:1.4:0.1. Lipid solutions of DSPC, cholesterol, DMG-PEG2000, and DSPE-PEG2000 in chloroform were evaporated at room temperature. The lipid film is redissolved in D-Lin-MC3 in ethanol. siRNA (Horizon Discovery) or ODN-1826 (Invitrogen) were resuspended in nuclease-free acetic acid buffer. Lipids were rapidly mixed with siRNA or ODN-1826 at a ratio of 1:3 (v/v). The solution was then probe sonicated at 20% PW at 30s on, 10s off cycles for a total of 8 cycles, 4min on. The solution was then dialyzed against nuclease-free PBS in 300kDa dialysis bags for 24 hours. Fluorescently tagged nanoparticles were made the same way, with the addition of 0.5 mol% DiR' (DiIC18(7)) (ThermoFisher). 0.5 mol% was taken away from cholesterol.

LNP characterization

Nanoparticles were analyzed for hydrodynamic size using DLS (Brookhaven Instruments) and zeta potential

(Anton Parr) in PBS. Drug loading was determined using Quant-it Ribo-green or Oli-green kits (ThermoFisher). Nanoparticles were first lysed open using a 1% Triton-X 100 solution. Dual-loaded nanoparticles were incubated with thermolabile exonuclease I (New England BioLabs) or RNase (ThermoFisher) for analysis of siRNA or CPG loading, respectively. Wells were analyzed using a plate reader (BioTek).

In vitro analysis

VISTA silencing capabilities in vitro were analyzed using flow cytometry. RAW264.7 macrophages (ATCC) were seeded in six-well plates with 5 mL of DMEM media (Gibco) supplemented with 10% fetal bovine serum (FBS, Cytiva) and 1% Penicillin-Streptomycin (Gibco). Cells were treated dual-LNPs, VISTA siRNA only LNPs at 50 nMol concentration of siRNA, or PBS. Cells were incubated together for 24 hours and then harvested off plates with 0.25% trypsin (Gibco) and pipetting. Single-cell suspensions were stained with anti-VISTA BV421 clone MIH63 (Biolegend) and Calcein A.M (Invitrogen). Cell suspensions were then read with the BD Fortessa. Data were analyzed with FlowJo software. Proinflammatory cytokine secretion was evaluated with ELISA assays. RAW264.7 macrophages were seeded in 24 wells plates with complete DMEM and treated with dual-LNPs or PBS at a 3 µg/mL concentration of CPG. Supernatant was collected 24 hours following incubation. TNF-α, GM-CSF, and IL-12_{p40} secretion were tested with the ELISAMax Kit (Biolegend) and read with the Synergy HT plate reader (BioTek).

Animal studies

YUMM1.7 cancer cells were purchased from ATCC and cultured in DMEM:F12 (ATCC) supplemented with 10% FBS (Gibco) and 1% PS (Gibco). Primary tumor models were established in 7-week-old C57BL/6J female mice (Jackson Labs) via left flank intradermal injection with 300,000 cell in 30 µL incomplete DMEM:F12 media. Treatments for all groups were administered on days 8, 15, 22, and 29 post primary inoculation. Groups receiving siRNA or antibody were given additional treatments with just siRNA or antibody on days 11, 18, 25, and 32 post primary inoculation. Weights and tumor caliper measurement were taken at least every other day. Tumor volume was calculated as $(\text{length} \times \text{width}^2) / 2$, where length was the longest axis of the tumor, and the width was perpendicular to the length. Euthanization criteria was tumor volume greater than 1000 mm³ or a weight drop of 20% the original weight. Local rechallenge studies were conducted by injecting 150,000 YUMM1.7 cells in 30 µL incomplete DMEM:F12 media intradermally to the right flank in mice that fully cleared their original primary tumors. Naïve C57BL/6J mice served as the control for tumor growth. Mice were monitored as previously described.

B16F10 cells were purchased from ATCC and cultured in DMEM media (Gibco). Primary tumor models were established in 7-week-old female C57BL/6J mice with

intradermal injections of 50,000 cells in 20 µL. Dual-LNP treatment was administered on days 15, 22, 29, and 36 post primary inoculation. Dual-LNP mice also received VISTA siRNA-LNP on days 18, 25, 32, and 39 post primary inoculation. PBS-treated mice received equivalent volumes of PBS on all treatment days. Monitoring was performed as described previously. MC38 cells were purchased from ATCC and cultured in DMEM media (Gibco). Primary tumor models were established in 7-week-old female C57BL/6J mice with intradermal injections of 100,000 cells in 30 µL. Dual-LNP treatment was administered on days 8, 15, 22, and 29 post primary inoculation. Dual-LNP treated mice also received VISTA siRNA-LNP days 11, 18, 25, and 32 post primary inoculation. PBS-treated mice received equivalent volumes of PBS on all treatment days. Monitoring was performed as described previously. Local rechallenge studies were conducted by injecting 50,000 B16F10 or MC38 cells in 30 µL incomplete DMEM media intradermally to the right flank in mice that fully cleared their B16F10 or MC38 original primary tumors, respectively. Naïve C57BL/6J mice served as the control for tumor growth. Mice were monitored as previously described.

ELISA of tumor tissue

12 days following start of treatment, blood was collected retro-orbitally, and mice were sacrificed for tumor harvest. Blood plasma was separated via centrifugation at 1500 rpm for 20 min. Blood plasma was immediately frozen at -80°C. Tumor tissue was weighed, submerged in 10 mL of PBS and homogenized with the Qiagen tissue homogenizer. The samples were frozen at -80°C and went through three freeze thaw cycles before analysis. TNFα, IL2, IFNγ, and IL12p40 ELISAs were performed according to manufacturer instructions (Biolegend). Absorbance readings were measured with a plate reader (BioTek).

Safety studies

3 hours following treatment of B16F10 tumor-bearing mice with the dual-LNP intratumorally, PBS intratumorally, or VISTA mAb (2e9) and soluble CPG systemically, blood was collected retro-orbitally. 5 days, 12 days, and 19 days following the start of treatment of YUMM1.7 tumor-bearing mice, blood was collected retro-orbitally. YUMM1.7 tumor-bearing mice were all treated locally with either dual-LNP, PBS, or VISTA mAb (2e9) + soluble CPG. Plasma was separated via centrifugation at 500 g for 20 min. Blood plasma was immediately frozen at -80°C. Alanine transaminase (Abcam) and IL-12p70 (Invitrogen) ELISAs were performed according to manufacturer instructions and read with a plate reader (BioTek). IL-6 and TNF-α were performed using Luminex assays and performed by the CWRU Bioanalyte Core.

Flow cytometry processing

Blood was collected retro-orbitally. Mice were sacrificed and tumor, liver, spleen, or tumor-draining lymph node

(TDLN) were harvest depending on the study. Liver, spleen, and TDLNs were processed through 70 μ m nylon mesh cell strainers (Fisherbrand) via agitation with the flat end of 3 mL or 5 mL syringes (BD Syringe). Liver, spleen, and TDLN cell pellets were resuspended in DMEM media+1% FBS. Red blood cells in spleen and blood cell pellets via rounds of ACK lysing buffer (Gibco), and then resuspended in DMEM media. Tumors were first cut up and then digested with liberase (0.4 mg/mL, Roche) and DNase (0.2 mg/mL, Roche) for 20 min at 37°C. They were then passed through 70 μ m nylon mesh cell strainers and resuspended in DMEM media. If the tumors were used for stimulation studies, they were resuspended in sterile, complete RPMI (Gibco) supplemented with 10% FBS, 1% PS, and 5 mM 2- β -mercaptoethanol (Gibco). Single-cell suspensions were plated in 96 U bottom well plates (Grenier Bio-one). Cells were washed with buffer (PBS+0.5% FBS+EDTA). Cells were blocked with CD16/CD32 Fc Block (Biolegend or BD Bioscience) and then stained with specific fluorescent antibodies. Cells undergoing intracellular staining or nuclear staining were fixed in fixation buffer from intracellular staining or FOXP3 staining kits from ThermoFisher. They were permeabilized and blocked with 2% normal rat serum (Biolegend). Cells were then stained with antibodies specific for cytokines or transcription factors of interest. Following staining, all cells were resuspended in buffer. All cells were read with the BDFortessa. All samples were analyzed with FlowJo software.

Myeloid and T cell population phenotyping

Antibodies purchased from Biolegend include CD45 (clone 30-F11), CD11b (clone M1/70), CD11c (clone N418), F4/80 (clone BM8), MHCII (clone M5/114.14.2), CD80 (clone 16-10A1), CD86 (clone GL-1), CD200R (clone OX-110), CD206 (clone C086C2), Ly6C (clone HK1.4), Ly6G (clone 1A8), CD4 (clone GK1.5), CD8 (clone 53-6.7), TCF1 (clone 7F11A10), Tim-3 (clone RMT3-23), Granzyme B (clone QA16A02), IFN γ (clone XMG1.2), TNF α (clone MP6-XT22), VISTA (clone MIH63), and Fc Block. FOXP3 antibody was purchased from ThermoFisher (clone FJK-16s). Cells were counterstained with DAPI (BD Bioscience). DCs were identified as CD11b⁺CD11c⁺F4/80⁻. Macrophages were identified as CD11b⁺ F4/80⁺, CD11c⁺ or CD11c⁻. Proinflammatory M1-like macrophages had additional markers of CD80, CD86, or MHCII. Anti-inflammatory M2-like macrophages had additional markers of CD206 and CD200R. M-MDSCs were identified as CD11b⁺ CD11c⁻ Ly6G⁻ Ly6C^{hi}. Regulatory T cells were identified as CD45⁺ CD4⁺ CD8⁻ FOXP3⁺.

ELISPOT

YUMM1.7 cells were irradiated at 100 Gy. Cells were passed 1 day after irradiation and used 3 days after irradiation. C57BL6/J mice were inoculated with YUMM1.7 cells, per previously described methods and treated with dual-LNPs

(VISTA siRNA+CPG) following the standard treatment timeline. Cured mice were rechallenged on the opposite flank. An equal number of naïve controls were also inoculated with the same number of cells on the same flank as the rechallenged mice. 12 days following challenge, the mice were sacrificed and the TDLN and spleen were harvested. Organs were processed and stained into single-cell suspension. Cells were spun down and then resuspended at a concentration of 10⁷ cells/mL in MojoSort buffer (Biolegend). The suspensions were then divided into thirds. One-third was positively selected for CD4⁺ T cells using magnetic beads and the MojoSort magnet (Biolegend). One-third was positively selected for CD8⁺ T cells using magnetic beads and the MojoSort magnet. The last third was saved for flow cytometry validation.

Cells were seeded in ELISPOT kits for IFN- γ (CTL) or Granzyme B ELISPOT (R&D Systems) at a density of 300,000 effector cells (from spleen or lymph node) and 10,000 stimulant cells (irradiated YUMM1.7 cells). Cells incubated together for 18 hours. Plates were washed and processed per manufacturer instructions. Plates were imaged and counted with a CTL ELISPOT reader. Small samples of the positively selected samples and depleted samples were saved for flow cytometry validation of CD4 T cell or CD8 T cell isolation. These samples were stained with CD8 FITC (clone 53-6.7, Biolegend) and CD4 PE (clone RM4-4, Biolegend), counterstained with DAPI and read on the BD Fortessa.

T CELL EX VIVO STIMULATION

C57BL6/J mice were inoculated with 300k-600k YUMM1.7 tumor cells to allow for better tissue recovery in the treated mice. Mice were treated for two full rounds of treatment. Control mice remained untreated. Mice were sacrificed and primary tumors were harvested. Organs were processed per flow protocol in sterile conditions. The final cell pellet was resuspended in 1 mL of complete, sterile complete RPMI media. 100 μ L of the cell suspension was plated in sterile U-bottom 96 well plates (2 replicates per mouse). 100 μ L of anti-CD3 (clone 2C11, Biolegend) and 100 μ L of anti-CD28 (clone PV1, BioX-Cell) were added to each of the samples for final concentrations of 2.5 μ g/mL 2C11 and 1 μ g/mL PV-1. Cells were incubated at 37°C, 5% CO₂ for 15 hours. 1x Monesin (Biolegend) and 1x Brefeldin A (Biolegend) were added and then incubated for an additional 4.5 hours at 37°C, 5% CO₂. Cells were then spun down and stained via the standard surface staining for flow cytometry. Additionally, the samples were permeabilized and IFN- γ and TNF- α (Biolegend) were intracellularly stained. Samples were run same day with the BD Fortessa.

Statistics

Statistics were performed using GraphPad Prism. Data are represented as mean \pm SEM with individual data points. Unpaired t-tests, one-way analysis of variance (ANOVA), and two-way ANOVA tests were performed

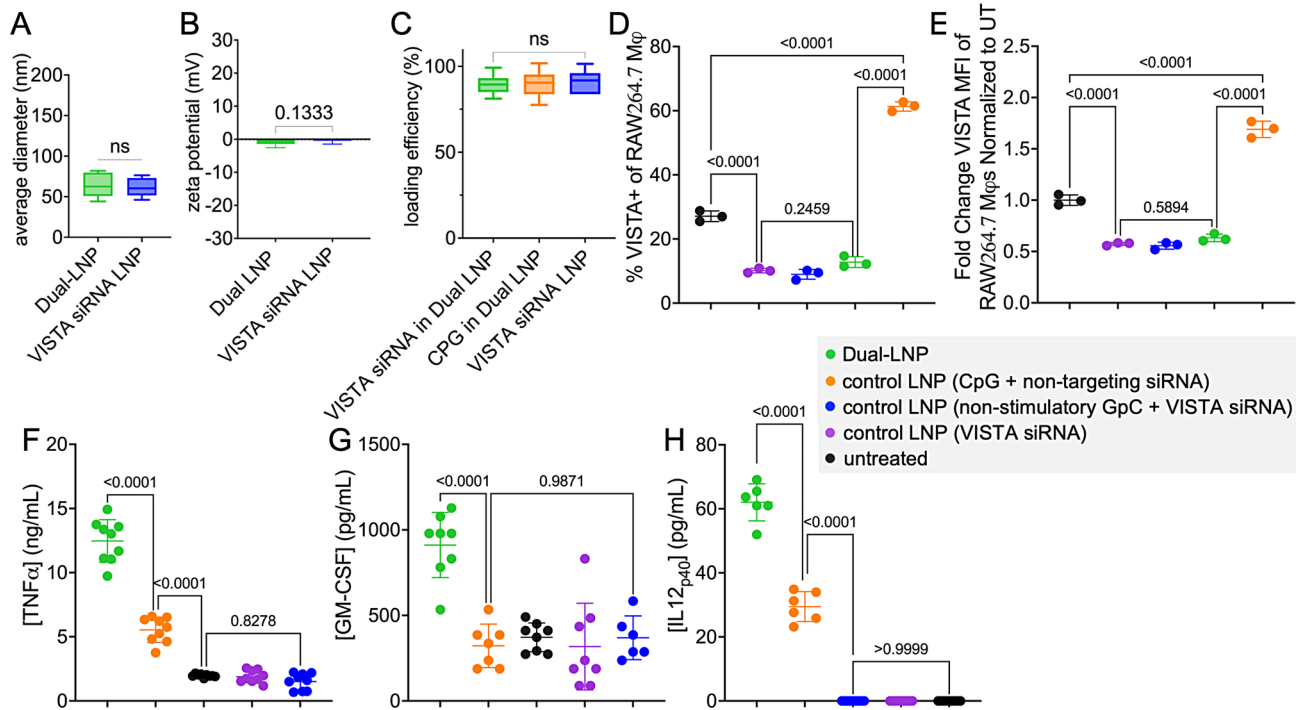


Figure 1 Characterization of the effects of dual LNP in vitro. (A) Hydrodynamic diameter of dual-LNP and VISTA siRNA only LNP. (B) Zeta potential of dual-LNP and VISTA siRNA only LNP. (C) Loading efficiency of siRNA or ODN-1826 CPG in the dual-LNP and control LNP loaded with VISTA siRNA only. RAW264.7 macrophages treated with dual LNP, control LNP (VISTA siRNA only), control LNP (CPG+non-targeting siRNA), control LNP (non-stimulatory GPC+VISTA siRNA), or PBS for 24 hours. (D) %VISTA⁺ cells. (E) VISTA expression (MFI) normalized to the untreated cells. Secreted cytokines, including TNF- α (F), GM-CSF (G), and IL-12_{p40} (H) were quantified by ELISA. Studies were conducted in independent triplicate and statistics were performed via Student's t-test or one-way ANOVA with Tukey's post-test. ANOVA, analysis of variance; LNP, lipid nanoparticle; VISTA, V-domain immunoglobulin suppressor of T cell activation; MFI, mean fluorescence intensity.

when required, with appropriate post-tests applied. Log-rank analysis was performed on median survival times. A $p < 0.05$ was considered significant.

RESULTS

Characterization of LNPs co-encapsulating VISTA-targeting siRNA and the TLR9 agonist CpG

The dual-LNP was synthesized by co-encapsulating ODN 1826 CpG Class B molecules and VISTA-targeting siRNA at a 2:5 ratio, a ratio that allows both efficient gene targeting and TLR9 activation in myeloid cells. We used ionizable cationic lipid D-Lin-MC3, cholesterol, DSPC, and poly-ethylene glycol (PEG) conjugated lipids. Under mild sonication for short periods of time, the LNPs formed by rapidly mixing the lipids with siRNA/CpG at pH 4. The dual-LNPs exhibited a very narrow size distribution (mean hydrodynamic diameter of 64.24 nm) with a zeta potential of -1.42 mV, indicating a nearly neutral surface charge (figure 1A,B). The efficiency of nucleotide loading into the LNP was shown by the encapsulation efficiency for CpG and VISTA siRNA as 89.61% and 89.55%, respectively (figure 1C). A comparison between the dual-LNP and the single-cargo LNP variants (only CpG or only VISTA siRNA) showed similar properties such as size, zeta potential and nucleotide encapsulation (online supplemental figure S1), indicating that the dual

cargo did not compromise the overall properties of the formulation.

CPG and VISTA siRNA co-encapsulating dual-LNP effectively downregulates the VISTA expression and upregulates the production of proinflammatory cytokines in vitro

The synergistic action of the dual-LNP was investigated in vitro using RAW264.7 macrophages. We also tested negative control dual-LNP formulations, which included LNPs encapsulating CpG and non-targeting siRNA or VISTA siRNA and GpC oligonucleotides (non-stimulatory CpG negative control molecule). The control LNP (VISTA siRNA) and control LNP (VISTA siRNA+non-stimulatory GPC) induced a twofold decrease in VISTA expression compared with the untreated cells, 24 hours following incubation (figure 1D,E). Representative VISTA expression histograms are shown in online supplemental figure S2. In contrast, the CPG containing LNP (CPG+scrambled siRNA) significantly upregulated VISTA expression following 24 hours of LNP incubation (figure 1D,E), revealing an immunosuppressive role of CPG and further justify the need to block VISTA. Importantly, the dual-LNPs that contain both CPG and VISTA-specific siRNA effectively ablated VISTA expression (figure 1D,E). Altogether, these data demonstrate the synergistic effect of VISTA siRNA and CPG co-encapsulation in downregulating VISTA expression.

Additionally, the stimulation capacity of the CPG ODN-1826 dinucleotide encapsulated within the dual-LNP was tested by evaluating the secretion of proinflammatory cytokines. After incubating the cells with LNPs for 24 hours, there was no significant cytokine secretion in cells treated with control LNP (VISTA siRNA alone) or control LNP (VISTA siRNA+non-stimulatory GPC) (figure 1F–H). Only when treated with the dual-LNP encapsulating both CPG and VISTA siRNA, significant cytokine secretion was observed (figure 1F–H). The dual-LNP induced a 2-fold increase in GM-CSF, 2.5-fold increase in TNF- α , and a 2-fold increase in IL-12_{p40} secretion compared with the control LNP (CPG+non-targeting siRNA) treatment. This data demonstrate that the addition of VISTA siRNA imparted synergistic effects on TLR-mediated stimulation and cytokine production. In summary, these studies have revealed that by co-encapsulating both CPG and VISTA-specific siRNA, the dual-LNP effectively silenced the VISTA protein expression and led to synergistic activation of cells following TLR stimulation.

IT administration of dual-LNP results in cellular uptake of LNPs by tumor-associated myeloid immune cells

The dual-LNPs were fluorescently labeled with DiR⁷ to assess their cellular uptake in the tumor, TDLN, blood, spleen, and liver using flow cytometry. The dual-LNPs were intratumorally injected in YUMM1.7 tumors in mice with the tumor size being about 60 mm³. The number of dual-LNP⁺ immune cells was significantly higher in the tumor than liver, spleen, TDLN, and blood (figure 2A). This indicates that intratumoral injection prevents the systemic distribution of LNPs, thereby potentially reducing the levels of systemic toxicity.

The dual-LNPs were primarily taken up by leukocytes, which is the main target cell population for the treatment (figure 2B). Within the tumor tissues, about 80% of all the dual-LNP⁺ live cells were CD45⁺ leucocytes. The majority of NP⁺ cells were also CD11b⁺ myeloid cells (~74%) (figure 2B). Specifically, the dual-LNP was found in ~89% of Ly6C^{hi} Ly6G⁺ monocytic MDSC (M-MDSC), ~70% of F4/80⁺ macrophages (M Φ), ~57% of CD11c⁺ DCs, and ~63% of Ly6C⁺ CD11c⁺ inflammatory DCs (figure 2C). The MFI of the DiR⁷ fluorescent tag was used to indicate the abundance of dual-LNP within the cells. CD11c⁺ DCs and the F4/80⁺ macrophages endocytosed the highest amount of dual-LNPs (figure 2D). Within the macrophage population, the M2-like anti-inflammatory cells endocytosed the highest amount of dual-LNP (figure 2E). Overall, this shows that dual-LNPs were primarily endocytosed by the phagocytic myeloid immune cells within the TME following IT injection. Representative flow cytometry dot plots illustrating the LNP⁺ gates on immune cells are shown in online supplemental figure S3.

After confirming that the distribution of dual-LNPs is mostly contained within the tumor volume, we investigated the short-term toxicity and systemic cytokine production in response to the intratumorally administered dual-LNP

in the B16F10 melanoma model. Control conditions included IT administration of phosphate-buffered saline (PBS), the systemic administration of VISTA-blocking mAb, and treatment of soluble CPG. After 1 dose of injection, the VISTA mAb and soluble CpG resulted in rapid elevation of the liver enzyme ALT and IL-12p70 in the blood, while the dual-LNP treatment produced baseline levels of ALT and IL-12p70 (figure 2F,G), suggesting the lack of systemic inflammation and the superior safety profile for the dual-LNP treatment. Next, we examined systemic cytokine release following the IT administration of dual-LNP versus the IT administration of VISTA-blocking mAb and soluble CPG in the YUMM1.7 melanoma model. Treatments were given weekly following the schedule and dosage that were used in the pilot studies for achieving effective therapeutic outcomes and were also followed for all studies described in the next sections. In terms of therapeutic efficacy, it should be noted that only the dual-LNP therapy was able to control and shrink tumors (online supplemental figure S4). Tumor sizes and animal weights are shown in online supplemental figure S4. All treatments initially showed basal levels of TNF- α and IL-6 in the blood (mediators of cytokine storm), 5 days following the start of treatment (figure 2H,K). However, the treatment with soluble CPG and VISTA-blocking mAb induced significantly higher levels of IL-6 in the blood halfway through treatment (12 days). Importantly, the dual-LNP-treated mice maintained baseline levels of systemic IL-6 and TNF- α at 12 days and 19 days following the start of treatment (figure 2I–K). These data suggest that the IT injection of dual-LNP generates limited systemic toxicities.

Dual-LNP therapy induces tumor regression

We tested the therapeutic efficacy of dual-LNP primarily the YUMM1.7 melanoma model for efficacy and mechanistic *in vivo* studies. The YUMM1.7 cells contain *Braf*^{V600E/wt}, *Cdkn2a*^{-/-}, and *Pten*^{-/-} genetic modifications, which are similar to the oncogenic mutations found in human melanoma.²⁹ Treatment began 8 days after inoculation, when the tumors reached a size of ~60 mm³. The dual-LNPs were intratumorally injected weekly for a total of 4 weeks at a dose containing 4 μ g of CPG and 10 μ g of VISTA siRNA. Treatment schedule is shown in online supplemental figure S5. To ensure continuous and sustained VISTA gene silencing, mice were injected with LNPs containing only VISTA-siRNA but devoid of CpG 3 days after every dual-LNP treatment. Control treatments followed the same schedule. PBS-treated control mice exhibited rapid tumor growth with a median survival of 30 days (figure 3A,B). The dual-LNP therapy significantly prolonged survival with a 47% cure rate. The non-complete responders from the dual-LNP-treated group significantly outlive the control mice, with a median survival of 43 days following inoculation (figure 3C,D). As a comparison, treatment with soluble CpG and VISTA mAb (clone 13F3) at a dose equivalent to the dual-LNP failed to induce any tumor regression,

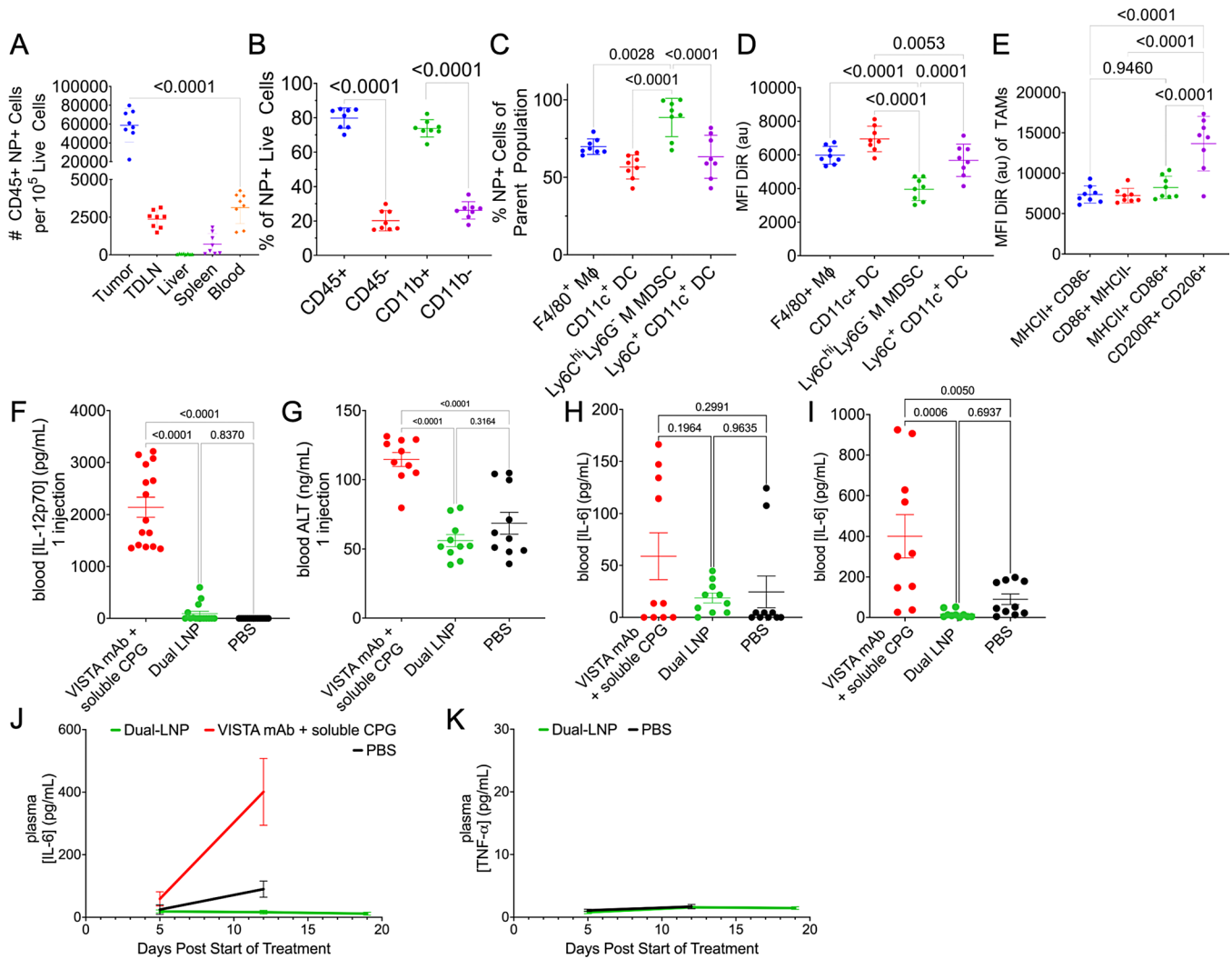


Figure 2 Studies of safety and biodistribution of dual LNP. Flow cytometry analysis of YUMM1.7 tumor tissues. (A) The number of CD45⁺ dual-LNP⁺ cells per 10⁵ live cells, (B) Percentages of CD45⁺, CD45⁻, CD11b⁺, CD11b⁻ cells among all dual-LNP⁺ cells, (C) Percentages of dual-LNP⁺ cells among each types of myeloid cells, including F4/80⁺ macrophages, CD11c⁺ total dendritic cells, Ly6C⁺ CD11c⁺ inflammatory dendritic cells, or Ly6C⁺ CD11c⁻ Ly6G⁻ M-MDSC populations, (D) Mean fluorescent intensity of dual-LNP DiR⁺ signal among the dual-LNP⁺ cell populations, and (E) Mean fluorescent intensity of dual-LNP DiR⁺ signal among the activated macrophage subset. (F) Blood IL-12_{p70} and (G) blood ALT enzyme levels were quantified following one dose of intratumorally administered dual-LNP, intratumorally administered PBS, or intravenously administered VISTA mAb and soluble CPG. Blood IL-6 concentration (H) 5 days following the start of treatment, (I) 12 days following the start of treatment, and (J) over several time points during treatment were shown. (K) Blood TNF-α concentration over several time points during treatment. Animal studies were performed with 5 mice per group. Statistics were analyzed by Student's t-test or one-way ANOVA with Tukey's post-test. ANOVA, analysis of variance; LNP, lipid nanoparticle; mAb, monoclonal antibody; MDSC, myeloid-derived suppressor cell; VISTA, V-domain immunoglobulin suppressor of T cell activation; PBS, phosphate-buffered saline.

yielding a median survival time of 29 days following inoculation (figure 3A,B). This indicates that the major advantage of dual-LNP is its high therapeutic potency at low and safe dose.

We also tested negative control LNP formulations, which included LNPs encapsulating CpG and non-targeting siRNA or VISTA siRNA and non-stimulatory GpC oligonucleotides. These negative control LNP formulations did not induce any regression in tumor growth (figure 3A). The median survival for the LNPs loaded with CpG and non-targeting siRNA was 29.5 days following inoculation and the median survival for the LNPs loaded with

GpC and VISTA siRNA was 25 days following inoculation (figure 3B). In fact, the survival of the mice treated with the control formulations was ~18 days shorter than that of the non-complete responders of the dual-LNP-treated group. The body weights of the groups are shown in online supplemental figure S6. These data indicate the dual-LNP treatment resulted in synergistic tumor control that relies on the codelivery of VISTA-targeting siRNA and the TLR9 agonist CpG into the same APCs.

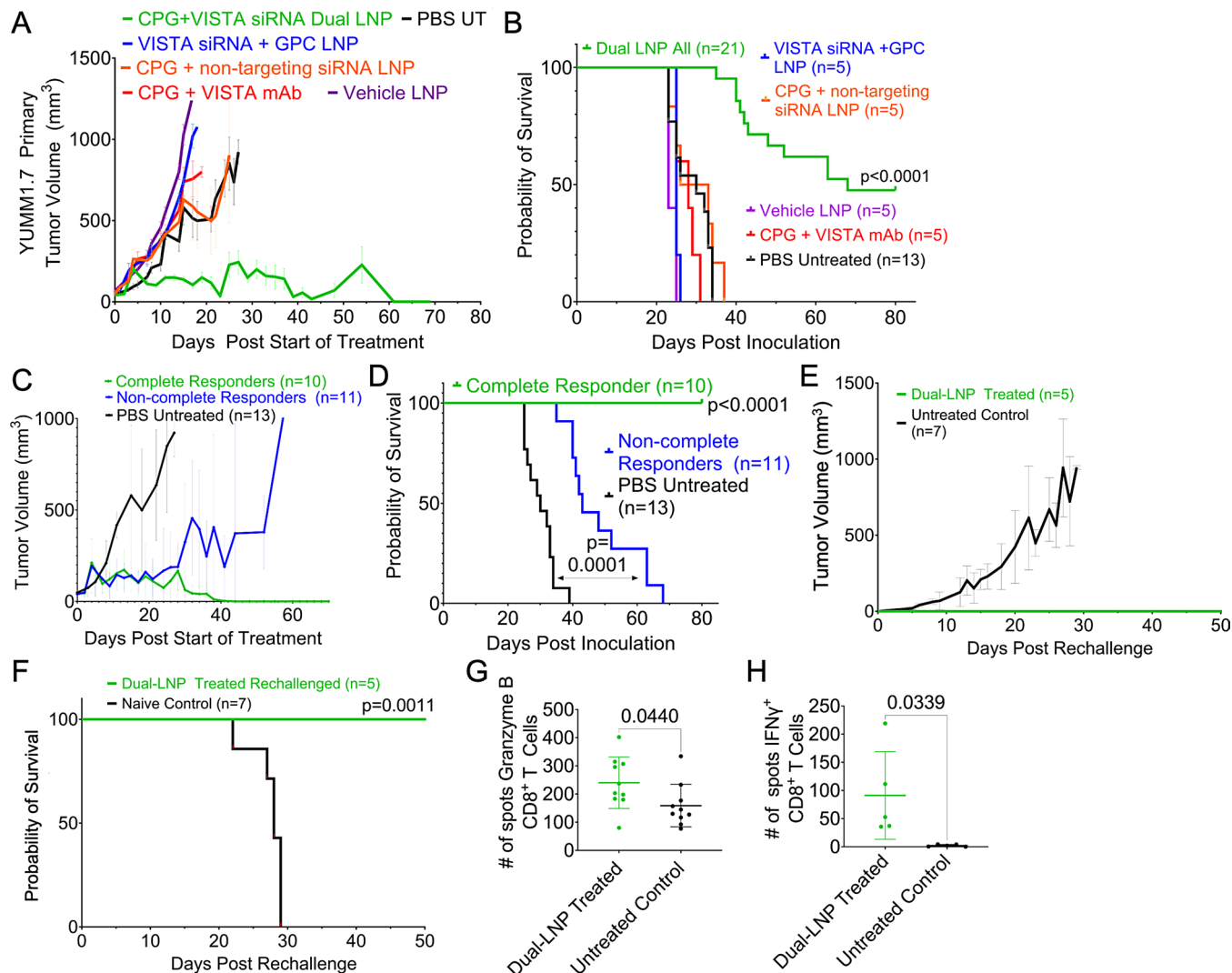


Figure 3 Survival study in the YUMM1.7 melanoma model in mice. Mice-bearing YUMM1.7 tumors were treated when the tumors were ~60 mm³. The dual-LNPs were injected intratumorally (IT) weekly for a total of 4 weeks at a dose containing 4 μ g of CPG and 10 μ g of VISTA siRNA. Mice were IT injected with VISTA-siRNA-only LNPs at a dose of a 10 μ g siRNA 3 days after a dual-LNP treatment. Similar schedule/dose were used for the control treatments. (A) Tumor growth curves for groups treated with dual LNP (n=21 mice), control LNP (VISTA siRNA+non-stimulatory GPC; n=5 mice), control LNP (CPG+non-targeting siRNA; n=5 mice), vehicle LNP (n=5 mice), CPG and VISTA mAb (n=5 mice), or PBS (n=13 mice). (B) Kaplan-Meier survival. (C) Tumor growth curves of the complete responders and non-complete responders in the dual-LNP-treated group. (D) Kaplan-Meier survival of complete and non-complete responders in the dual-LNP-treated group. (E) A subset of complete responders (n=5) was rechallenged with YUMM1.7 cells on their opposite flank 30 days after completion of the dual-LNP treatments. The tumor growth was compared with naïve controls (n=7). (F) Kaplan-Meier survival of rechallenged mice. A subset of complete responders (n=5) was used for ELISPOT assays. CD4 and CD8 T cells were isolated 12 days following rechallenge. T cells were stimulated with irradiated YUMM1.7 cells (100 Gy). (G) ELISPOT results for Granzyme B from lymphatic CD8⁺ T cells following rechallenge. (H) ELISPOT results for IFN- γ from splenic CD8⁺ T cells following rechallenge. Statistics were analyzed by Student's t-test. LNP, lipid nanoparticle; VISTA, V-domain immunoglobulin suppressor of T cell activation; PBS, phosphate-buffered saline.

Dual-LNP treatment elicits long-term immunological memory and prevention of recurrence

The complete responders following the dual-LNP treatment were rechallenged on their opposite flank 30 days following the last treatment. Naïve mice were inoculated with YUMM1.7 tumors as parallel controls. While the control mice all grew tumors and had a median survival of 28 days, 100% of the rechallenged mice rejected their tumors (figure 3F,G). The tumor rejection is likely driven by T cells developed and sustained within the treated

mice. To measure the frequency of antigen-specific T cells, we used the ELISPOT assay (online supplemental figure S7). CD8⁺ T cells from the TDLN (rechallenge tumor site) were stimulated with irradiated YUMM1.7 cells. Granzyme B-specific ELISPOT assay was performed to enumerate the number of activated CD8⁺ T cells. Our results showed that a significantly higher number of CD8⁺ T cells from dual-LNP-treated mice produced Granzyme B when compared with the untreated controls (figure 3H). Similarly, IFN- γ ELISPOT analysis using splenic CD8⁺ T

cells stimulated with irradiated YUMM1.7 cells showed a 42-fold higher number of spots in the LNP-treated mice than the untreated controls (figure 3I). ELISPOT plate images are shown in online supplemental figure S7.

Dual-LNP silences VISTA and alters tumor-infiltrating myeloid immune cell populations

To assess how the dual-LNPs affect the tumor immune microenvironment at an earlier time point that preceded tumor regression, we investigated the tumor-associated myeloid cells 5 days after treatment initiation. We tested the control LNPs that contained VISTA siRNA and non-stimulatory GPC or non-targeting siRNA and CPG. Within the tumor tissues, the total CD45⁺ immune cells nearly doubled in all LNP-treated tumors, compared with saline-treated mice (figure 4A). Notably, the total CD11b⁺ myeloid cells were significantly increased by treatment with both control LNP formulations (figure 4B). Representative flow plots immune cells breakdown in dual-LNP treated and PBS treated tumors are shown in online supplemental figure S8.

Among the myeloid populations, only the dual-LNP-treated tumors exhibited a significant decrease in the immunosuppressive subsets and an increase in the activated proinflammatory APCs. Importantly, all LNP treatments reduced the abundance of immunosuppressive M-MDSCs (figure 4C, D). While saline-treated mice maintained an M-MDSC population that made up 12.66±4.18% of CD11b⁺ cells, dual-LNP treatment ablated the M-MDSC population to 0.40%±0.23% (figure 4E). Previous studies have suggested that tumor-associated M-MDSCs are immature progenitor cells that are capable of differentiating into predominantly macrophages in a permissive environment.³⁰ We found that the dual-LNP treatment induced an accumulation of Ly6C⁺ CD11c⁺ DCs, (a 7.3x increase from 4% to 30%) (figure 4F,G). Although control LNP treatments also reduced M-MDSCs from the TME, the control treatments failed to expand the inflammatory DC population the same way the dual-LNP treatment did (figure 4F). This result supports the hypothesis that only the combination of CPG and VISTA siRNA in the dual-LNP induced the differentiation of the M-MDSCs into inflammatory DCs.

In addition, the dual-LNP treatment significantly reduced VISTA protein expression while enhancing MHCII expression in tumor-associated myeloid populations. In the dual-LNP treated group, the percentage of VISTA⁺ CD11c⁺ F4/80⁻ DCs dropped significantly from 58% in saline-treated tumors to 44% (figure 4H). The control LNP (VISTA siRNA+non-stimulatory GPC) treatment also significantly decreased VISTA expression in DCs. On the other hand, the MHCII⁺ DCs were only increased in response to the dual-LNP treatment (by a remarkable 34-fold) (figure 4I). Compared with all the controls, the dual-LNP treatment resulted in a 2-fold decrease in VISTA⁺ macrophages (figure 4J,K) and a 3.3-fold increase in the MCHII⁺ macrophage population (figure 4L and M). Treatment with both types of control

LNPs failed to diminish VISTA expression in macrophages. However, both types of control LNPs increased MHCII expression in the macrophages compared with saline-treated tumors, although significantly less than the dual-LNP therapy. Thus, the unique ability of dual-LNP to enhance the maturation of both DCs and macrophages may lead to improved tumor antigen presentation and better stimulation of tumor-specific T cells. Importantly, these effects of dual-LNP are attributed to the codelivery of CPG and VISTA-targeting siRNA to the same APC cell,

Dual-LNP induces the activation of myeloid APCs in the TDLN

Tumor-specific T cells are initially primed in the TDLN, where migratory DCs and macrophages migrate from the tumor tissues and present tumor-associated antigens to cognate T cells.³¹ We hypothesize that the dual-LNP treatment induces the maturation of APCs that migrate to the TDLN, which in turn result in better priming of tumor-specific T cells. Thus, we investigated the phenotypes of TDLN APCs and T cells following treatment with dual-LNP, control LNP (VISTA siRNA+non-stimulatory GPC), control LNP (CPG+non-targeting siRNA), or PBS saline. Representative flow cytometry dot plots are shown in online supplemental figure S9, showing myeloid cell gating of dual-LNP treated and PBS-treated mice. At the early time point (5 days following treatment initiation), myeloid cell populations were significantly expanded in the TDLN, with a 1.5x increase in all LNP treated conditions compared with the untreated group (figure 5A). Dual-LNP treatment induced a significantly higher number of DCs (figure 5B) than the PBS-treated mice or either control-LNP treated mice. The dual-LNP treatment also induced an accumulation of monocytes (figure 5C and D) compared with all control treated tumors. T cells in the TDLN showed the most significant expansion, with a 3.42-fold increase in CD4⁺ T cells (figure 5E and F) and a 7.35-fold increase in CD8⁺ T cells following dual-LNP treatment compared with saline-treated mice (figure 5G and H). The groups treated with control LNP (VISTA siRNA+non-stimulatory GPC) and control LNP (CPG+non-targeting siRNA) also exhibited T cell expansion within the TDLN. Altogether, these results demonstrate that the dual-LNP therapy induces an accumulation of activated DCs in the TDLN that lead to better priming and expansion of tumor-reactive cytotoxic T cells.

In addition to the early time point, we also examined TDLN following the second round of treatment. Our data show that the trend of myeloid cell influx was maintained at this later time point. Representative flow cytometry gating is shown in online supplemental figure S9. At a later time point (12 days after treatment initiation), the TDLN in dual-LNP-treated mice had twofold higher number of CD11b⁺ myeloid cells than untreated mice (online supplemental figure S10A). The number of CD11c⁺ DCs (online supplemental figure S10B) was significantly increased compared with the untreated group. The number of F4/80⁺ macrophages was significantly increased compared

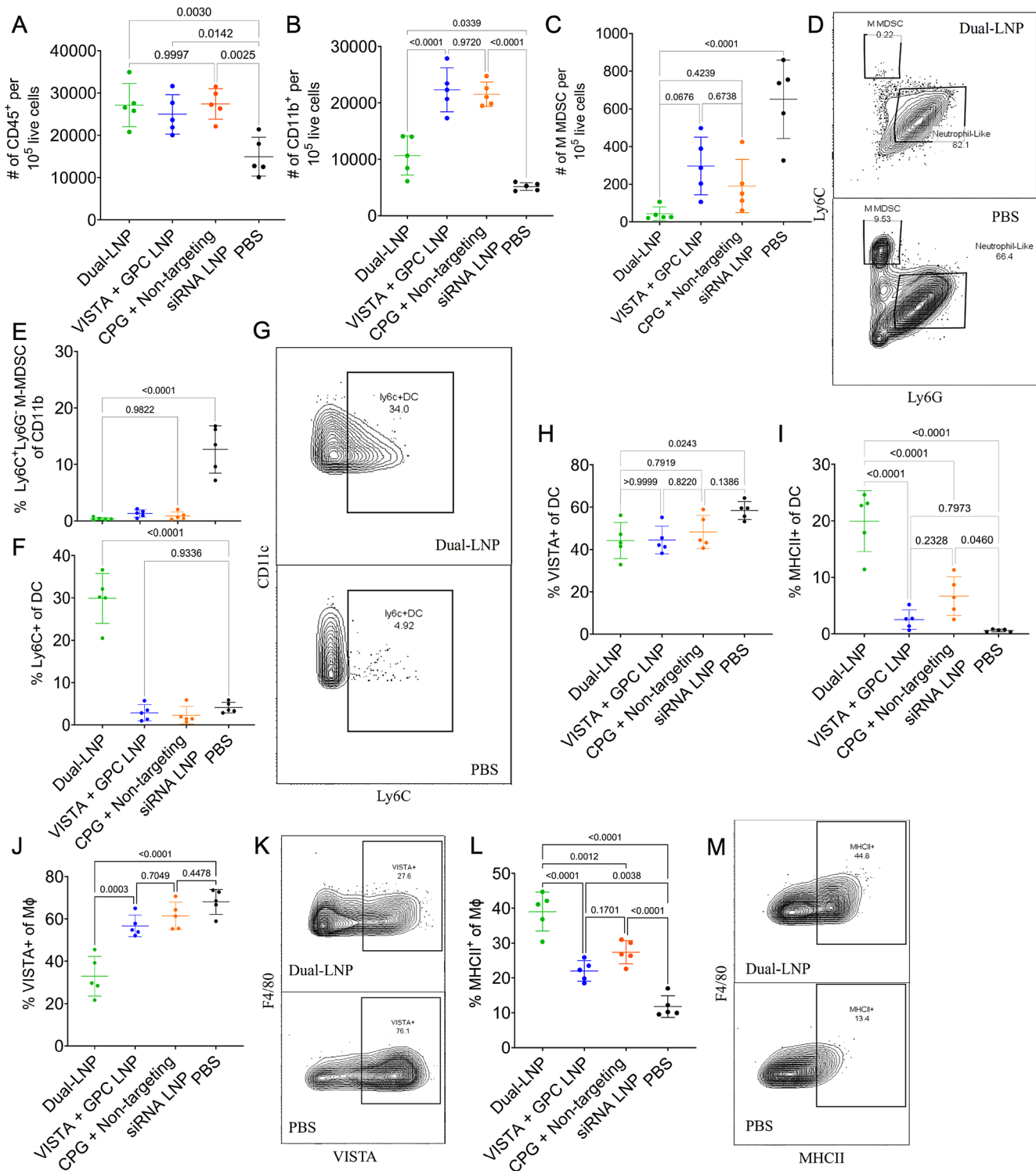


Figure 4 Myeloid immune cell profile of primary YUMM1.7 tumors 5 days after the initiation of the dual-LNP treatment. Mice were treated with dual-LNP, control LNP (VISTA siRNA+non-stimulatory GPC), control LNP (CPG+non-targeting siRNA), or saline. Tissue was harvested 5 days after the start of treatment. The number of (A) CD45⁺ immune cells and (B) CD11b⁺ immune cells per 10⁵ live cells in the tumor microenvironment. (C) The number of M-MDSC cells in the tumor microenvironment per 10⁵ live cells. (D) Representative flow plot of MDSC populations in dual-LNP and PBS-treated mice. (E) The percentage of CD11b⁺ myeloid immune cells that are M-MDSCs. (F) % of DCs that are Ly6C⁺. (G) Representative flow plots of Ly6C⁺ expression in DC populations for dual-LNP treated and PBS-treated mice. (H) % of DCs that are VISTA⁺. (I) % of DCs that are MHCII⁺. (J) % of Mφs that are VISTA⁺. (K) Representative flow plots of VISTA expression in Mφ from dual-LNP treated and PBS-treated mice. (L) % of Mφs that are MHCII⁺. (M) Representative flow plots of MHCII expression in Mφ from dual-LNP treated and PBS-treated mice. All experiments were performed with five mice per group. Statistics were analyzed by one-way ANOVA with Tukey's post-test. ANOVA, analysis of variance; DCs, dendritic cells; LNP, lipid nanoparticle; MDSC, myeloid-derived suppressor cell; VISTA, V-domain immunoglobulin suppressor of T cell activation; PBS, phosphate-buffered saline.

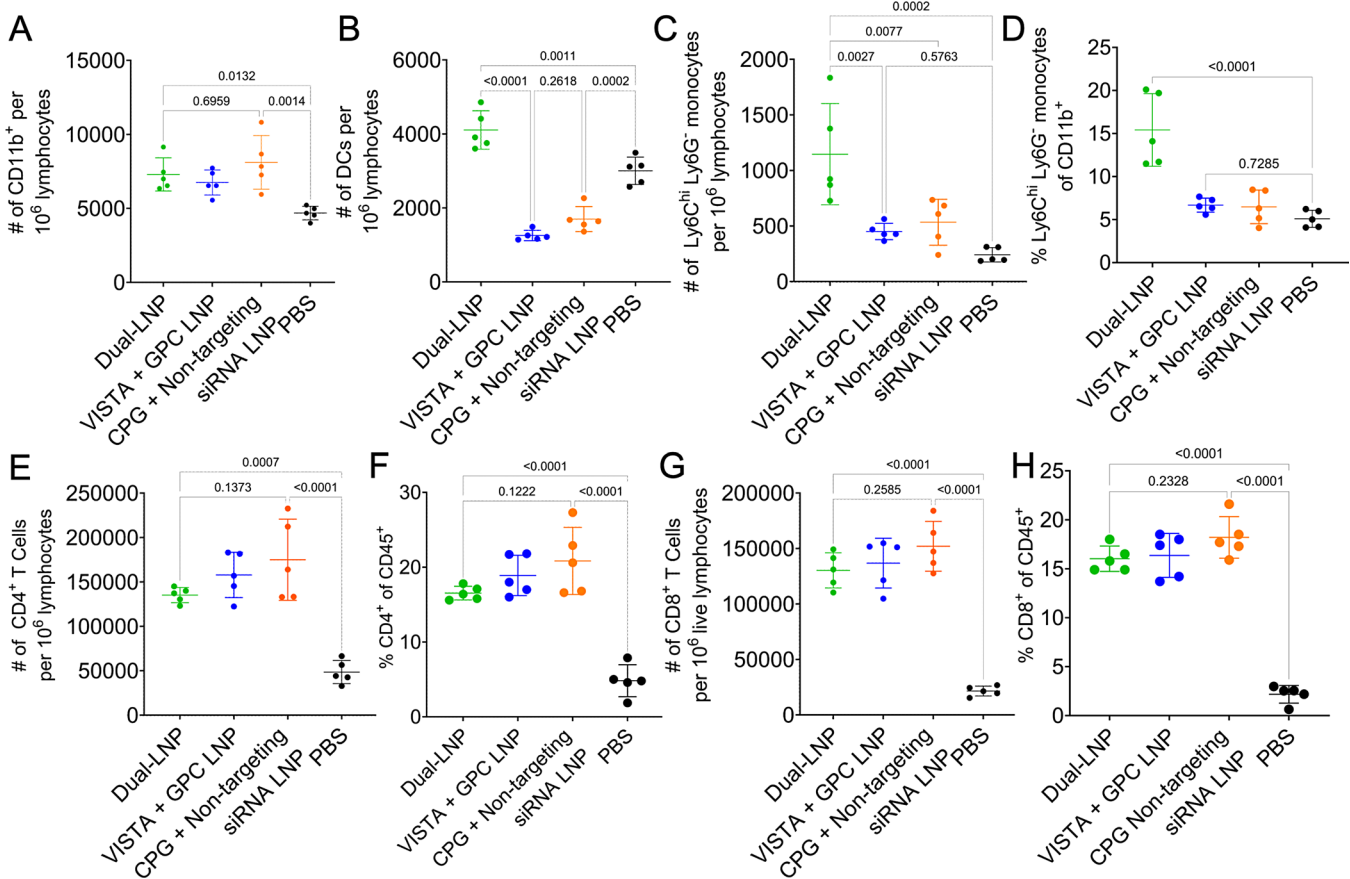


Figure 5 Myeloid immune cell profile of the tumor-draining lymph node 5 days after the initiation of the dual-LNP treatment. Flow cytometry analysis 5 days after treatment initiation with dual-LNP, control LNP (VISTA siRNA+GPC), or control LNP (CPG+non-targeting siRNA). (A) The number of CD11b⁺ myeloid immune cells per 10⁶ lymphocytes. (B) The number of DCs per 10⁶ lymphocytes. (C) The number of monocytes cells per 10⁶ lymphocytes. (D) The percentage of CD11b⁺ myeloid immune cells that are monocytes. (E) The percentage of CD45⁺ immune cells that are CD4⁺ T cells. (F) The number of CD4⁺ T cells per 10⁶ lymphocytes. (G) The percentage of CD45⁺ immune cells that are CD8⁺ T cells. (H) The number of CD8⁺ T cells per 10⁶ lymphocytes. All experiments were performed with five mice per group. Statistics were analyzed by one-way ANOVAs with Tukey's post-test. ANOVA, analysis of variance; LNP, lipid nanoparticle.

with the untreated group (online supplemental figure S10C). Within macrophages, we examined activation markers CD80 and CD86 in conjunction with MHC class II expression. The percentage of macrophages that express MHCII and CD80 or CD86 are significantly higher in TDLN of mice treated with dual-LNP compared with the PBS control (online supplemental figure S10D-F). Altogether, these results indicate that dual-LNP therapy induces an influx of activated DCs and macrophages in TDLN, which contribute to the efficient priming of tumor-reactive T cells.

Dual-LNP treatment augments the cytotoxic activity of tumor-infiltrating CD8⁺ T cells

Based on the findings in the TDLN, we postulate that a large population of tumor-specific T cells were expanded and migrate to tumor tissues following dual-LNP treatment. We examined the phenotypes and functional status of tumor-infiltrating lymphocytes (TILs) at 12 days following the treatment. We found that the number of CD45⁺ immune cells was

significantly increased in the tumors (online supplemental figure S11A) while the VISTA expression on CD45⁺ immune cells remained significantly down-regulated (online supplemental figure S11B). Additionally, there was a significant expansion of TCF1⁺ Tim3⁻ progenitor of exhausted subsets (T_{pex}) in both CD4⁺ and CD8⁺ T cells in dual-LNP treated tumors compared with untreated tumors. The percentage of TCF1⁺ Tim3⁻ CD4⁺ T_{pex} cells exhibited a 5-fold increase within the dual-LNP treated tumors (online supplemental figure S11C) while the CD8⁺ T_{pex} cells showed 2–3 fold of increase (online supplemental figure S11D). Representative flow cytometry plots are shown in online supplemental figure S12. Additionally, the dual-LNP treated tumor tissues maintained a more proinflammatory state as evidenced by the significantly higher levels of IFN- γ , TNF- α , IL-12p40, and IL-2 compared with mock-treated tumors (online supplemental figure S11E–H).

To investigate the effector function of CD8⁺ TILs after the treatments, we isolated TILs and ex

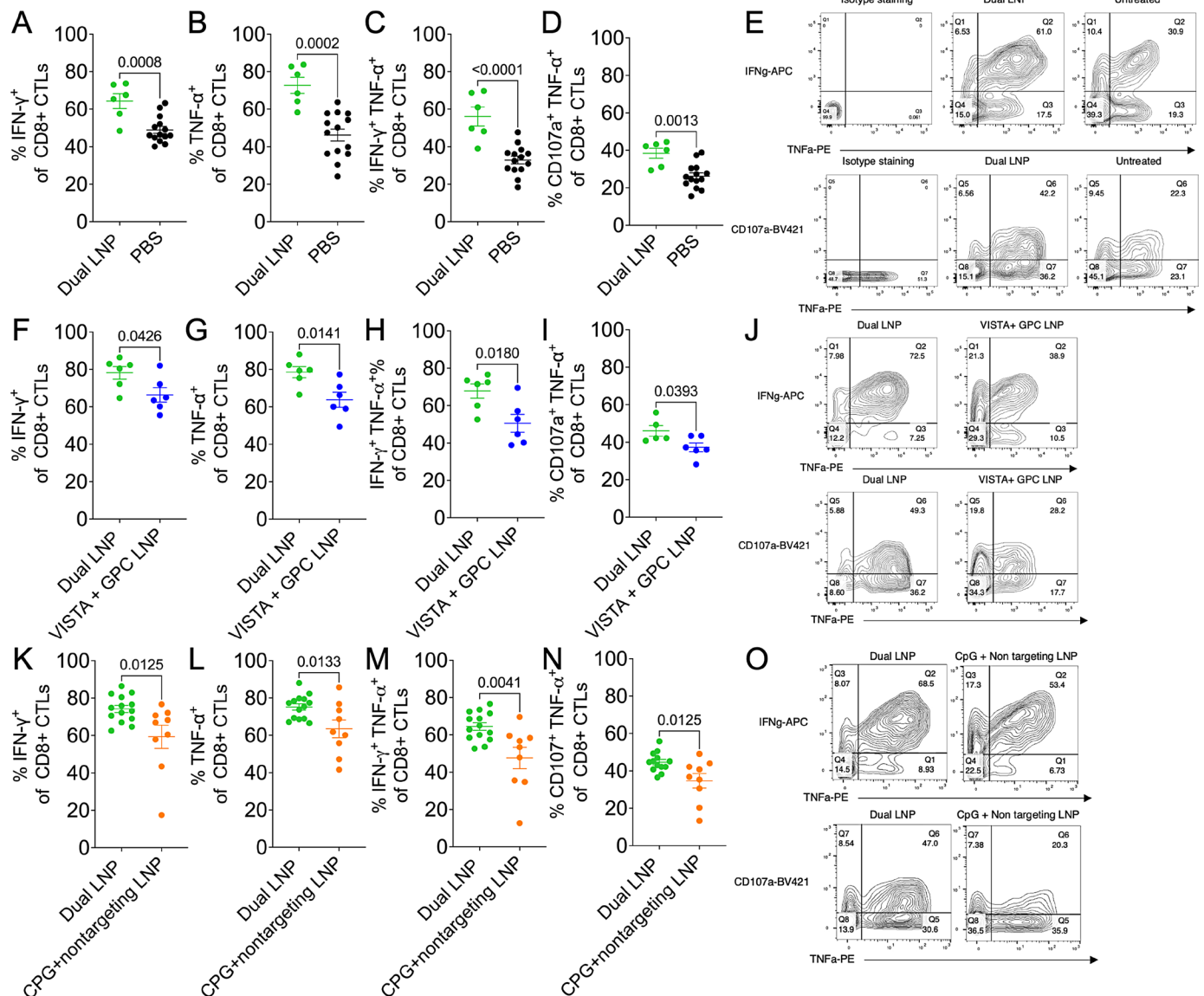


Figure 6 The superior effector function of CD8 $^+$ tumor-infiltrating T cells following treatment with dual-LNP. Mice were inoculated with YUMM1.7 tumors and treated with either PBS, dual-LNP, VISTA control dual-LNP (VISTA siRNA-non-stimulatory GPC), and CPG control dual-LNP (CPG+non-targeting siRNA). (A–E) Tumors were harvested 12 days after the start of treatment with dual-LNP and PBS treated. Tumor-associated lymphocytes were stimulated ex vivo with antiCD3 and antiCD28 for 16 hours. The expression of effector molecules was examined by flow cytometry and shown as the percentages of CD8 $^+$ TILs. The percentages of IFN- γ^+ (A), TNF- α^+ (B), IFN- γ^+ TNF- α^+ (C), and CD107a $^+$ TNF- α^+ (D), CD8 $^+$ TILs in dual-LNP and PBS-treated tumors were shown. (E) Representative flow cytometry plots of IFN- γ , TNF- α , and CD107a staining. (F–J) Tumors were harvested and stimulated 14 days after the start of treatment with dual-LNP and control LNP (VISTA siRNA+non-stimulatory GPC). IFN- γ^+ (F), TNF- α^+ (G), IFN- γ^+ TNF- α^+ (H), and CD107a $^+$ TNF- α^+ (I), CD8 $^+$ TILs in dual CPG+VISTA siRNA LNP and PBS-treated tumors were shown. (J) Representative flow cytometry plots of IFN- γ , TNF- α , and CD107a staining. (K–O) Tumors were harvested and stimulated 14 days after the start of treatment with dual LNP and control LNP (CPG+non-targeting siRNA). IFN- γ^+ (K), TNF- α^+ (L), IFN- γ^+ TNF- α^+ (M), and CD107a $^+$ TNF- α^+ (N), CD8 $^+$ TILs in dual CPG+VISTA siRNA LNP and PBS-treated tumors were shown. (O) Representative flow cytometry plots of IFN- γ , TNF- α , and CD107a staining. All experiments were performed with at least six mice per group. Statistics were analyzed by Student's t-test. LNP, lipid nanoparticle; VISTA, V-domain immunoglobulin suppressor of T cell activation; PBS, phosphate-buffered saline.

vivo stimulated with anti-CD3 and anti-CD28. The dual-LNP significantly increased the polyfunctional cytokine-producing CD8 $^+$ TILs cells as evidenced by higher percentages of IFN- γ^+ , TNF- α^+ , and IFN- γ^+ TNF- α^+ subsets when compared with untreated tumors, or tumors treated with control LNP (VISTA

siRNA+non-stimulatory GPC) or control LNP (CPG+non-targeting siRNA) (figure 6). Additionally, CD107a $^+$ TNF- α^+ CD8 $^+$ T cells were identified to indicate active degranulation. Consistently, CD8 $^+$ TILs from tumors treated with the dual-LNP showed higher percentages of CD107a $^+$ TNF- α^+ CD8 $^+$ T compared

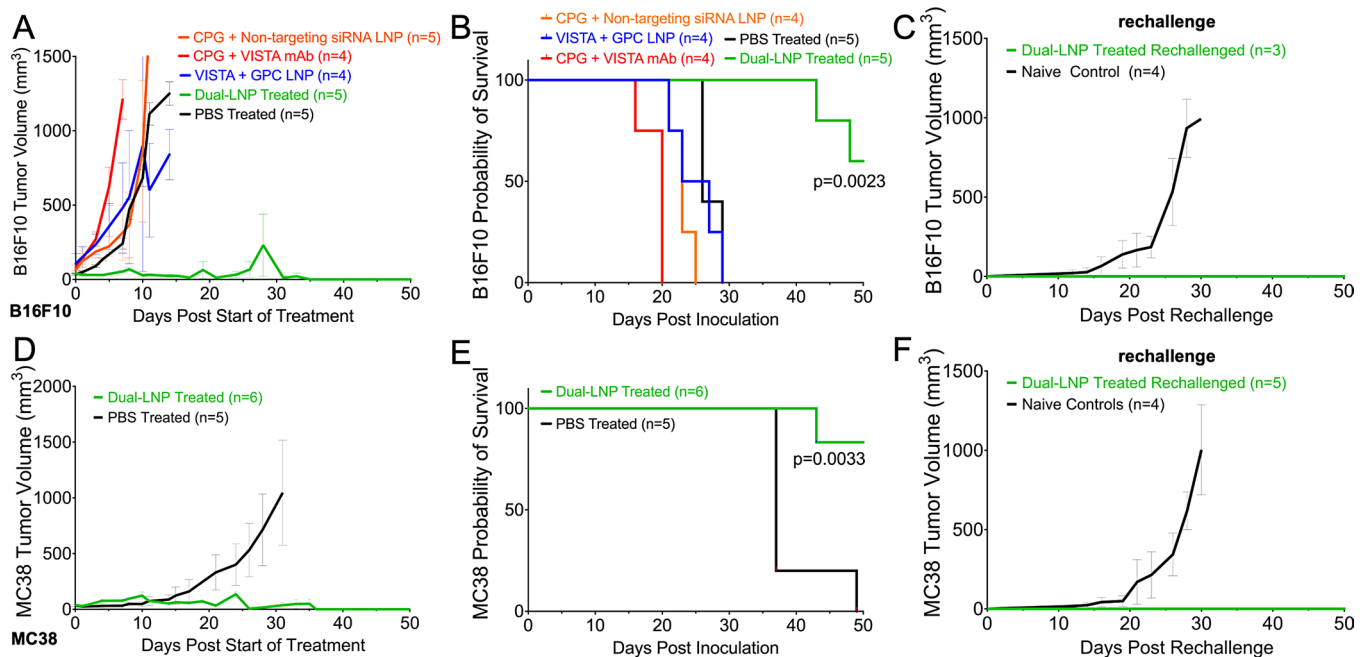


Figure 7 Survival of B16F10 and MC38 tumor-bearing mice. Mice bearing a B16F10 tumor or MC38 tumor were treated starting 15 days or 8 days after inoculation, respectively, when the tumors were ~60 mm³. The dual-LNPs were injected intratumorally (IT) weekly for a total of 4 weeks at a dose containing 4 μg of CPG and 10 μg of VISTA siRNA. Mice were IT injected with VISTA-siRNA-only LNPs at a dose of a 10 μg siRNA 3 days following every dual-LNP treatment. Similar schedule and dose were used for the control treatments. (A) B16F10 tumor growth curves for groups treated with dual-LNP, control LNP (VISTA siRNA+non-stimulatory GPC), control LNP (CPG+non-targeting siRNA), VISTA mAb and soluble CPG, or PBS (n=4–5 per group). (B) Kaplan-Meier survival of B16F10 tumor-bearing mice. (C) B16F10 tumor growth curves following tumor rechallenge of the complete responders treated with dual-LNP. The rechallenge experiment was conducted with the three complete responders and four naïve control mice. (D) MC38 tumor growth curves for groups treated with dual-LNP or PBS (n=6 for the dual LNP-treated group; n=5 for the PBS control group). (E) Kaplan-Meier survival of MC38 tumor-bearing mice. (F) MC38 tumor growth curves following tumor rechallenge of the complete responders treated with dual-LNP. The rechallenge experiment was conducted with five complete responders and four naïve control mice. LNP, lipid nanoparticle; VISTA, V-domain immunoglobulin suppressor of T cell activation; PBS, phosphate-buffered saline.

with untreated mice or mice treated with control LNPs. Representative flow cytometry plots of cytokine staining and CD107a expression are shown in figure 6E, J and O. Altogether, these results indicated that dual-LNP treatment synergistically augmented the effector function of tumor-reactive CD8⁺ cytotoxic T cells that mediate tumor clearance (figure 3A).

The dual-LNP therapy controls tumor growth in the B16F10 melanoma model and MC38 colon cancer model

Next, we examined the therapeutic effects of dual-LNP in two additional tumor models. The same dose and schedule of the dual-LNP treatment was employed for mice bearing B16F10 or MC38 tumors. The median survival of the untreated B16F10 mice was 26 days post inoculation (figure 7A). Similarly to the YUMM1.7 tumor-bearing mice, B16F10 tumor-bearing mice also had uncontrollable tumor growth in response to the control LNP treatments (CPG+non-targeting siRNA or VISTA siRNA+non-stimulatory) (figure 7A and B). Additionally, treatment with soluble CPG and VISTA mAb (clone 2e9) also failed to control tumor growth (figure 7A and B). However, the dual-LNP treatment produced significant therapeutic benefits in B16F10

melanomas as indicated by control over tumor growth (figure 7A). Treatment of B16F10 melanoma tumors with the dual-LNP induced a 60% cure rate (figure 7B). The complete responders were rechallenged on their opposite flank 30 days following the last treatment. Naïve mice with B16F10 tumors served as controls. While the B16F10 untreated control mice all grew tumors and had a median survival of 26 days, 100% of the B16F10 complete responder, rechallenged mice rejected their tumors (figure 7C). A similar trend was seen in the MC38 tumor model (figure 7D). The median survival of the untreated MC38 tumor-bearing mice was 37 days post inoculation (figure 7E). The dual LNP treatment led to tumor clearance in 83% of the treated group. The body weights of the groups are shown in online supplemental figure S13. All MC38 complete responders were rechallenged with the same tumor cells and showed complete protection while naïve controls all succumbed to tumor burden (figure 7F). The high cure rates in both B16F10 and MC38 models as well as protection against tumor regrowth validated the results from the YUMM1.7 model and indicate the utility of dual-LNP in treating



multiple types of cancers. The robust development of memory response indicates that the dual-LNP therapy not only controls the growth of primary tumors but also imparts long-term protection and prevents tumor recurrence.

DISCUSSION

In this work, we have assessed the dual-LNP vaccine targeting a critical immune checkpoint protein VISTA for cancer immunotherapy. We developed a stable and reproducible LNP codelivering CpG and VISTA-specific siRNA. Using multiple preclinical models, we have demonstrated the multipotency of the dual-LNPs in stimulating anti-tumor immunity, by simultaneous delivery of two immunostimulatory cargoes into APCs, direct reprogramming of tumor-associated myeloid cells, activation of DC and macrophages that in turn prime tumor-specific T cells, augmenting the effector function of CTLs, and promoting memory T cell responses. These multimodal effects collectively led to potent therapeutic benefits at a safe low dose without inducing any visible systemic inflammation. Mechanistically, the dual-action nanoparticle leverages the simultaneous immune activation by TLR9 stimulation with silencing the gene expression of VISTA. VISTA has been shown to regulate TLR signaling in myeloid cells and controlling myeloid cell-mediated immunosuppression.¹⁹ Consequently, the dual-LNP reprograms myeloid cell-mediated innate immune responses within the TME.

Intratumorally injected dual-LNPs were predominantly taken up by tumor-associated myeloid cells, including MDSCs, M2 TAMs and DCs. Thus, the dual-LNP ensures the uptake of both cargoes by the same APCs. One significant advantage of the dual-LNP is the sequestration in the tumor tissues, which decreased its 'spill' into blood circulation, thus lowering the likelihood of systemic toxicity. Local administration of dual-LNP offers significant advantages including direct antitumor immune response within the primary tumor, improved peripheral immunosurveillance and reduced systemic irAE. Despite the enormous excitement associated with the highly promising results of VISTA inhibition in preclinical studies, the first human trial of a VISTA-blocking mAb was prematurely terminated (NCT02671955) due to systemic irAE.³² Similarly, soluble TLR agonists, if injected via systemic route, will trigger systemic inflammatory responses that may be highly toxic. Our studies show that the Dual-LNP resulted in minimal systemic level of inflammation, in comparison to soluble TLR9 agonist or VISTA-specific mAb treatment, thereby offering safety advantages.

In addition to the safety profile, the dual-LNP offers potent therapeutic benefits. By simultaneously delivering two cargoes to the immunosuppressive myeloid cells, the dual-LNP can effectively reprogram the immunosuppressive TME to a highly T cell-stimulatory TME. Studies from murine models^{12,17} and human cancers have shown high VISTA expression in tumor tissues, such as in melanoma,³³ colon cancer, ovarian,³⁴ oral squamous cell.

and pancreatic.³⁶ Thus, we postulate that the dual-LNP will directly target tumor-associated myeloid cells to induce potent antigen presentation. Indeed, we observed the rapid (within 5 days following the dual-LNP treatment) and nearly complete elimination of the M-MDSC population in the TME. The reduction of MDSCs was also seen following treatment of VISTA-blocking mAb, although with moderate level of reduction compared with the dual-LNP treatment.¹⁹ A significant connection can be observed between an overall decrease in VISTA expression on myeloid cells and increased activity of CD4⁺ T cells and CD8⁺ T cells in the tumor, affirming the role of VISTA as a myeloid cell-specific immune checkpoint protein. In conclusion, IT treatment with dual-LNP directly targets tumor-associated myeloid cells by simultaneously reducing VISTA expression and inducing the expansion and activation of DCs and macrophages. This results in a sustained T cell activation and the development of systemic memory responses that are critical for long-term tumor remission.

Author affiliations

¹Department of Biomedical Engineering, Case Western Reserve University, Cleveland, Ohio, USA

²Department of Translational Hematology and Oncology Research, Cleveland Clinic, Cleveland, Ohio, USA

³Department of Molecular Medicine, Cleveland Clinic Lerner College of Medicine, Case Western Reserve University School of Medicine, Cleveland, Ohio, USA

⁴Case Comprehensive Cancer Center, Cleveland, Ohio, USA

Acknowledgements We acknowledge the Bioanalyte Core, Case Comprehensive Imaging Core, Cytometry and Imaging Microscopy Core, and Radiation Resources Core at the Comprehensive Cancer Center of Case Western Reserve University and University Hospitals of Cleveland.

Contributors TJM: conceptualization, data curation, formal analysis, validation, investigation, visualization, methodology, writing—original draft, writing—review and editing. HMT: formal analysis, validation, investigation, methodology, writing—original draft, writing—review and editing. AB: investigation, data curation, methodology. KEP: investigation, methodology. DWH: investigation, methodology. GMA: investigation, methodology. ASC: investigation, methodology. MGH: investigation, methodology. LO: investigation, methodology. MD: investigation, methodology. LLW: conceptualization, supervision, funding acquisition, writing—review and editing. EK: conceptualization, supervision, funding acquisition, writing—review and editing. All authors have read and approved this article. LLW and EK are responsible for the overall content as the guarantors.

Funding This work was supported by grants from the National Cancer Institute R01CA253627 (EK), R01CA278633 (EK and LLW), P30CA043703 (EK), R01CA223804 (LLW), R21CA258618 (LLW), the Department of Defense CDMRP W81XWH-21-MRP-MCAA ME210229 (LLW) and CDMRP W81XWH-21-LCRP-IITRA LC210336 (LLW), the American Cancer Society RSG-18-045-01-LIB (LLW), and the Angie Fowler AYA Cancer Research Fund (EK). TJM was supported by the NSF graduate research fellowships program. AB was supported by a fellowship from the NIH Interdisciplinary Biomedical Imaging Training Program (T32EB007509).

Competing interests LLW is an inventor involved with the commercial development of VISTA with ImmuNext (Lebanon, NH). The other authors declare no potential conflicts of interest.

Patient consent for publication Not applicable.

Ethics approval All animal studies were performed under an approved protocol (protocol 2016-0115) by the Institutional Animal Care and Use Committee at Case Western Reserve University.

Provenance and peer review Not commissioned; externally peer reviewed.

Data availability statement All data relevant to the study are included in the article or uploaded as online supplemental information.

Supplemental material This content has been supplied by the author(s). It has not been vetted by BMJ Publishing Group Limited (BMJ) and may not have been peer-reviewed. Any opinions or recommendations discussed are solely those of the author(s) and are not endorsed by BMJ. BMJ disclaims all liability and responsibility arising from any reliance placed on the content. Where the content includes any translated material, BMJ does not warrant the accuracy and reliability of the translations (including but not limited to local regulations, clinical guidelines, terminology, drug names and drug dosages), and is not responsible for any error and/or omissions arising from translation and adaptation or otherwise.

Open access This is an open access article distributed in accordance with the Creative Commons Attribution Non Commercial (CC BY-NC 4.0) license, which permits others to distribute, remix, adapt, build upon this work non-commercially, and license their derivative works on different terms, provided the original work is properly cited, appropriate credit is given, any changes made indicated, and the use is non-commercial. See <http://creativecommons.org/licenses/by-nc/4.0/>.

ORCID iD

Efstathios Karathanasis <http://orcid.org/0000-0001-7484-7552>

REFERENCES

- Schreiber RD, Old LJ, Smyth MJ. Cancer immunoeediting: integrating immunity's roles in cancer suppression and promotion. *Science* 2011;331:1565–70.
- Demaria O, Cornen S, Daéron M, et al. Harnessing innate immunity in cancer therapy. *Nat New Biol* 2019;574:45–56.
- Wang J, Li D, Cang H, et al. Crosstalk between cancer and immune cells: Role of tumor-associated macrophages in the tumor microenvironment. *Cancer Med* 2019;8:4709–21.
- Veglia F, Perego M, Gabrilovich D. Myeloid-derived suppressor cells coming of age. *Nat Immunol* 2018;19:108–19.
- Joyce JA, Fearon DT. T cell exclusion, immune privilege, and the tumor microenvironment. *Science* 2015;348:74–80.
- Roy D, Gilmour C, Patnaik S, et al. Combinatorial blockade for cancer immunotherapy: targeting emerging immune checkpoint receptors. *Front Immunol* 2023;14.
- Sharma P, Allison JP. The future of immune checkpoint therapy. *Science* 2015;348:56–61.
- Postow MA, Callahan MK, Wolchok JD. Immune Checkpoint Blockade in Cancer Therapy. *J Clin Oncol* 2015;33:1974–82.
- Wang L, Rubinstein R, Lines JL, et al. VISTA, a novel mouse Ig superfamily ligand that negatively regulates T cell responses. *J Exp Med* 2011;208:577–92.
- Xu W, Hiêu T, Malarkannan S, et al. The structure, expression, and multifaceted role of immune-checkpoint protein VISTA as a critical regulator of anti-tumor immunity, autoimmunity, and inflammation. *Cell Mol Immunol* 2018;15:438–46.
- Flies DB, Han X, Higuchi T, et al. Coinhibitory receptor PD-1H preferentially suppresses CD4⁺ T cell-mediated immunity. *J Clin Invest* 2014;124:74589:1966–75.
- Johnston RJ, Su LJ, Pinckney J, et al. VISTA is an acidic pH-selective ligand for PSGL-1. *Nature* 2019;574:565–70.
- Teft WA, Kirchoff MG, Madrenas J. A molecular perspective of CTLA-4 function. *Annu Rev Immunol* 2006;24:65–97.
- Hui E, Cheung J, Zhu J, et al. T cell costimulatory receptor CD28 is a primary target for PD-1-mediated inhibition. *Science* 2017;355:1428–33.
- Wang L, Le Mercier I, Putra J, et al. Disruption of the immune-checkpoint VISTA gene imparts a proinflammatory phenotype with predisposition to the development of autoimmunity. *Proc Natl Acad Sci U S A* 2014;111:14846–51.
- Le Mercier I, Chen W, Lines JL, et al. VISTA Regulates the Development of Protective Antitumor Immunity. *Cancer Res* 2014;74:1933–44.
- Liu J, Yuan Y, Chen W, et al. Immune-checkpoint proteins VISTA and PD-1 nonredundantly regulate murine T-cell responses. *Proc Natl Acad Sci U S A* 2015;112:6682–7.
- Ta HM, Roy D, Zhang K, et al. LRIG1 engages ligand VISTA and impairs tumor-specific CD8⁺ T cell responses. *Sci Immunol* 2024;9:eadi7418.
- Xu W, Dong J, Zheng Y, et al. Immune-Checkpoint Protein VISTA Regulates Antitumor Immunity by Controlling Myeloid Cell-Mediated Inflammation and Immunosuppression. *Cancer Immunol Res* 2019;7:1497–510.
- Schaafsma E, Croteau W, ElTanbouly M, et al. VISTA Targeting of T-cell Quiescence and Myeloid Suppression Overcomes Adaptive Resistance. *Cancer Immunol Res* 2023;11:38–55.
- Zhang K, Zakeri A, Alban T, et al. VISTA promotes the metabolism and differentiation of myeloid-derived suppressor cells by STAT3 and polyamine-dependent mechanisms. *Cell Rep* 2024;43:113661.
- Deng J, Li J, Sarde A, et al. Hypoxia-Induced VISTA Promotes the Suppressive Function of Myeloid-Derived Suppressor Cells in the Tumor Microenvironment. *Cancer Immunol Res* 2019;7:1079–90.
- Martins F, Sofiya L, Sykiotis GP, et al. Adverse effects of immune-checkpoint inhibitors: epidemiology, management and surveillance. *Nat Rev Clin Oncol* 2019;16:563–80.
- Das SK, Menezes ME, Bhatia S, et al. Gene Therapies for Cancer: strategies, Challenges and Successes. *J Cell Physiol* 2015;230:259–71.
- Wang Y, Zhang L, Xu Z, et al. mRNA Vaccine with Antigen-Specific Checkpoint Blockade Induces an Enhanced Immune Response against Established Melanoma. *Mol Ther* 2018;26:420–34.
- Marin-Acevedo JA, Soyano AE, Dholaria B, et al. Cancer immunotherapy beyond immune checkpoint inhibitors. *J Hematol Oncol* 2018;11:8.
- Jayaraman M, Ansell SM, Mui BL, et al. Maximizing the potency of siRNA lipid nanoparticles for hepatic gene silencing in vivo. *Angew Chem Int Ed Engl* 2012;51:8529–33.
- Kulkarni JA, Witzigmann D, Leung J, et al. On the role of helper lipids in lipid nanoparticle formulations of siRNA. *Nanoscale* 2019;11:21733–9.
- Meeth K, Wang JX, Micevic G, et al. The YUMM lines: a series of congenic mouse melanoma cell lines with defined genetic alterations. *Pigment Cell Melanoma Res* 2016;29:590–7.
- Kwak T, Wang F, Deng H, et al. Distinct Populations of Immune-Suppressive Macrophages Differentiate from Monocytic Myeloid-Derived Suppressor Cells in Cancer. *Cell Rep* 2020;33:108571.
- Mellman I, Chen DS, Powles T, et al. The cancer-immunity cycle: Indication, genotype, and immunotype. *Immunity* 2023;56:2188–205.
- Wu C, Cao X, Zhang X. VISTA inhibitors in cancer immunotherapy: a short perspective on recent progresses. *RSC Med Chem* 2021;12:1672–9.
- Kuklinski LF, Yan S, Li Z, et al. VISTA expression on tumor-infiltrating inflammatory cells in primary cutaneous melanoma correlates with poor disease-specific survival. *Cancer Immunol Immunother* 2018;67:1113–21.
- Liao H, Zhu H, Liu S, et al. Expression of V-domain immunoglobulin suppressor of T cell activation is associated with the advanced stage and presence of lymph node metastasis in ovarian cancer. *Oncol Lett* 2018;16:3465–72.
- Wu L, Deng W-W, Huang C-F, et al. Expression of VISTA correlated with immunosuppression and synergized with CD8 to predict survival in human oral squamous cell carcinoma. *Cancer Immunol Immunother* 2017;66:627–36.
- Blando J, Sharma A, Higa MG, et al. Comparison of immune infiltrates in melanoma and pancreatic cancer highlights VISTA as a potential target in pancreatic cancer. *Proc Natl Acad Sci U S A* 2019;116:1692–7.